ChemPubSoc Europe

DOI: 10.1002/slct.201600355

Chemistry SELECT Full Papers

Electro, Physical & Theoretical Chemistry

Synchrotron based operando surface X-ray scattering study towards structure–activity relationships of model electrocatalysts

Andrey Goryachev,[a] Francesco Carlà,[b] Jakub Drnec,[b] Willem G. Onderwaater,[b, c] Roberto Felici,[b, d] Philipp P. T. Krause,[e] Ad H. Wonders,[a] Emiel J. M. Hensen,*[a] and Jan P. Hofmann*[a]

A novel combination of Surface X-ray Scattering techniques (SXS), i.e. GISAXS (Grazing-Incidence Small-Angle X-Ray Scattering), XRR (X-Ray Reflectivity) and SXRD (Surface X-Ray Diffraction) alongside with simultaneous detection of gaseous products by OLEMS (On-Line Electrochemical Mass Spectrometry) has been applied to study under *operando* conditions structure-activity relationships of a Pt model electrocatalyst. The SXS-OLEMS combination is able to follow dynamic changes in surface morphology and crystallography during water electrolysis. To showcase the combined SXS-OLEMS setup for *operando* studies of electrode transformations, H_2 and O_2 evolution reactions (HER and OER) on a Pt model electrocatalyst and their dependence on type and degree of surface roughening have been investigated.

Introduction

Efficient electrocatalysts for water splitting are a crucial ingredient to the successful implementation of chemical energy conversion for the storage of intermittently available renewable energy in the form of gaseous or liquid fuels. In the last decades, many spectroscopic and microscopic techniques have been adapted and developed by electrochemists to study the multi-electron processes occurring on electrode surfaces as well as to track changes in surface composition, structure, and morphology. EC-STM (Electrochemical Scanning Tunneling Microscopy), LEED (Low-Energy Electron Diffraction) and AES (Auger Electron Spectroscopy) are examples of those commonly accepted surface science techniques adapted for electrochemistry.[1–8] However, LEED and AES require ultra-high vacuum (UHV) conditions to operate and involve sample transfer from liquid electrolyte to UHV, which increases the chance of contamination and induces changes in the sample environment. Additionally, potential dependent changes on the surface (such as formation of intermediates or new layers) can be only recorded *in-situ* under electrochemical conditions by means of e.g. EC-STM, Raman and infrared spectroscopy, or ellipsometry.[9–13] All above-mentioned techniques yield insight into one structural or compositional (chemical) property at the time. Structure-activity relations can only be directly determined by probing simultaneously the catalytic activity of the catalyst material, e.g. in form of gaseous product formation by means of mass spectrometry, and the structure by *in-situ* techniques.

Recent developments of synchrotron based *in-situ* methods enable the study of processes, which were impossible or only very difficult to study by lab-based techniques. The advantage of using hard X-ray radiation in studying electrochemical systems lies mostly in the small absorption cross section of light elements which are the principal constituents of aqueous electrolytes (*cf.* Figure S2). Having polymer (e.g. PEEK) *in-situ* cells with thin, X-ray transparent walls available, allows simultaneous collection of structural (surface or bulk crystallography, roughness) and chemical (layer composition) information.[14,15] Specular XRR (X-Ray Reflectivity) has been commonly used to study (multi)layered thin film systems and gives access to surface roughness and film thickness by probing density profiles perpendicular to the surface.[16–18] Unlike ellipsometry, XRR does not require preliminary information of the sample, such as refractive indices, and retains the signal intensity even in presence of electrolyte as an advantage of using hard X-rays. GISAXS (Grazing Incidence Small Angle Scattering) measurements

[a] *A. Goryachev, A. H. Wonders, Prof. E. J. M. Hensen, Dr. J. P. Hofmann*
Laboratory of Inorganic Materials Chemistry
Department of Chemical Engineering and Chemistry
Eindhoven University of Technology
P.O. Box 513, 5600MB Eindhoven, The Netherlands
E-mail: e.j.m.hensen@tue.nl
j.p.hofmann@tue.nl
[b] *Dr. F. Carlà, Dr. J. Drnec, W. G. Onderwaater, Dr. R. Felici*
European Synchrotron Radiation Facility
71 Avenue des Martyrs, 38000 Grenoble, France
[c] *W. G. Onderwaater*
Huygens-Kamerlingh Onnes Laboratory
Leiden University
P.O. Box 9504, 2300 RA Leiden, The Netherlands
[d] *Dr. R. Felici*
CNR-SPIN
Area della Ricerca di Roma 2 - "Tor Vergata"
Via del Fosso del Cavaliere 100, I- 00133 Roma, Italy
[e] *P. P. T. Krause*
Physikalisch-Chemisches Institut
Justus-Liebig-Universität Gießen
Heinrich-Buff-Ring 58, 35392 Gießen, Germany

Supporting information for this article is available on the WWW under http://dx.doi.org/10.1002/slct.201600355

© 2016 Wiley-VCH Verlag GmbH & Co. KGaA, Weinheim

can be utilized for following surface morphological changes such as island formation.[5,8–20] As GISAXS probes very small wave vector transfer (Q) values both perpendicular and parallel to the surface, it is sensitive to structures with periodicity between a few nm and a few hundreds of nm. SXRD (Surface X-Ray Diffraction) and CTR (Crystal Truncation Rods) provide surface specific information on both composition and crystallography.[21–23] The combination of all three SXS techniques (XRR, GISAXS, SXRD) allows to investigate surface structural changes of both crystalline and non-crystalline features ranging over different periodicity regimes.

To study the catalytic performance of the model electrode in an *operando* manner, we used common electrochemical analysis (chronoamperometry, cyclic voltammetry) and an On-Line Electrochemical Mass-Spectrometry (OLEMS) system designed and developed by Wonders *et al.*[24] OLEMS allows for nearly instantaneous gas-through-liquid detection of gaseous products by means of a porous Teflon-modified PEEK capillary connected to a quadrupole mass-spectrometer via a differentially pumped inlet system.[25–28] The mass spectrometric detection of electrolysis products adds chemical information to the electrochemically measured current at a given potential by identification of (gaseous) product molecules. This additional information is especially of interest, when reactions with a selectivity dimension are studied.

By combining both synchrotron-based X-ray structural characterization and OLEMS we have a unique tool at hand, which enables us to track activity and selectivity trends and directly relate them to structural changes of an electrode surface. To introduce the approach, we have chosen as a showcase hydrogen and oxygen evolution reactions (HER and OER, respectively) on a Pt(111) single crystal electrode featuring a high stability and activity in HER.[29–31] Moreover, the fact that the system has been studied for more than 30 years makes Pt(111) an ideal model catalyst to validate the proposed combined SXS-OLEMS approach.

Related electrocatalytic studies have shown that Pt(111) undergoes partial surface reconstruction under applied bias.[1,2,32] Potential cycling in acidic electrolytes leads to formation of Pt islands mostly composed of (110) and (100) facets[2] resulting in an increased H_2 evolution activity. On the other hand, repeated polarization of the Pt surface with OER pulses to high positive potentials leads to the formation of core-shell like Pt-PtO_x structures resulting in partial Pt dissolution along with a loss in HER activity.[32–36]

Results and Discussion

Roughening by fast potential cycling

In the cyclic voltammograms of the roughened surface, one can observe the formation of reversible features at +0.26 V, +0.20 V and +0.05 V corresponding to underpotential adsorption of hydrogen on Pt(100), (110) and (111) facets followed by a sharp cathodic peak of H_2 evolution starting at 0.00 V (Figure 1a).[4] On the positive side of the plot, a noticeable anodic peak corresponding to O_2 evolution starts to appear at +1.56 V

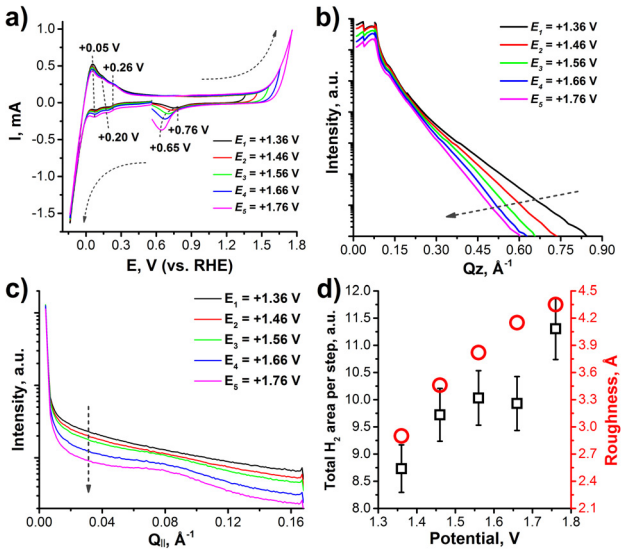

Figure 1. a) Cyclic voltammograms of the roughened Pt model electrode recorded at 50 mV/s, dashed arrows show scan direction; b) specular XRR plots of the electrode surface taken after every roughening step; c) line scans of GISAXS patterns taken along the maximum intensity change recorded after every roughening step (2D GISAXS pattern are reported in Figure S6 b–f); d) amount of H_2 evolved per potential step vs. maximum applied upper (OER) potential in the roughening CVs and corresponding roughness parameter.

preceded by Pt oxidation starting at about +0.70 V (*cf.* also Figure S4b). Sweeping back to cathodic direction reveals an oxide reduction peak (ORP) at about +0.76 V, which appears even in the case of low upper potentials E_{OER} = +1.36 V and +1.46 V. Moreover, increasing E_{OER} of the roughening CV sequence leads to a negative shift of the ORP position by 110 mV accompanied by an increase of the ORP peak area. Unlike minor changes in the HER region, a noticeable negative shift of the ORP peak might be explained by formation of a thick Pt oxide at high potentials.[37,38] Along with oxidation, surface reconstruction of the Pt model electrode occurs as fast potential cycling results in the partial rearrangement of (111) facets into (100) and (110) facets, which might lead to changes in the HER activity (Figure 1d).[4] Moreover, the surface oxide is more stable on the reconstructed surface containing (100) and (110) facets rather than on bare Pt(111).[39,40]

A decrease in XRR intensity for $Q_z > 0.20$ Å^{-1} caused by the applied CV sequences points to changes in the surface roughness (Figure 1b). Quantitative fitting of the re-integrated XRR curves shows an increase of the surface roughness (σ) from 2.90 Å to 4.35 Å for the roughening steps E_N = +1.36 V and E_N = +1.76 V, respectively (Figure S5, Table S1). The decrease of GISAXS intensity, similar to that observed in XRR, further corroborates surface roughening by the applied potential cycling sequences. (Figure 1c). A feature appearing at $Q_{||}$ = 0.08 Å^{-1} in the GISAXS line scans recorded after potential cycling with E_{OER} higher than +1.56 V corresponds to the formation of Pt islands with an average inter-island distance of about 7.8 nm.[1] Another indication of surface roughening is the decrease of the (111) reflex as observed by SXRD (Figure S4c). The total amount of

© 2016 Wiley-VCH Verlag GmbH & Co. KGaA, Weinheim

hydrogen evolved per step increased by 24% (Figure 1d), which is consistent with the increase in the surface area as a result of the change of surface morphology and change of the reaction rates due to the faceting of the surface.

Surface roughening by potential pulsing followed by *operando* XRR-OLEMS

Unlike the relatively slow potential sweeping during cyclic voltammetry, actual electrochemical devices (such as fuel cells and electrolyzers) operate in a constant potential/current mode. A working electrode subjected to a constant positive or negative potential might undergo deactivation by partially irreversible surface oxidation.[33,41,42] In order to investigate structural differences induced by either fast (potential pulsing) or slow (potential cycling) surface roughening, a sequence of repeated pulses of E_{OER} (+1.86 V, 10 s) and E_{HER} (−0.14 V, 10 s) potentials with intermittent resting potential E_{RES} (+0.56 V, 10 s) has been applied to a UHV cleaned Pt model electrode (Figure S1c).

In an attempt to track fast surface changes, the way of recording XRR data was speeded up by fixing the angular position of the incident beam and detector at $Q_z = 0.4$ Å^{-1}, where a maximum intensity change has been observed in the XRR scan (Figure 1b) in the previous experiment. As a result, so-called continuous 1-point XRR plots have been recorded during potential pulsing. Simultaneously, the OLEMS signal of $m/z = 2$ (H_2) and $m/z = 32$ (O_2) have been acquired to evaluate the HER and OER activities of the Pt electrode in an *operando* manner.

The XRR plot reveals two reflectivity domains with low and high reflectivity upon switching between OER (+1.86 V) and HER (–0.14 V) potentials, respectively (Figure 2a). Under positive potential (E_1) the reflectivity instantly drops 1.5 times compared to negative (E_3) and resting potentials (E_2, E_4). Changing back to the resting potential (E_2) leads to a reflectivity increase with a noticeable induction period of 2–4 s at the beginning of each potential pulse alluding to the slow kinetics of surface relaxation and surface oxide reduction.[5,43] Further decrease of the potential towards HER (E_3) followed by applying a resting potential (E_4) leads only to a slight reflectivity drop (< 0.8%) upon applying the HER potential. This may be related to H adsorption on the electrode surface. The H_2 production rate is also decreasing with time and reaches a plateau after 9 pulse cycles. Unlike in HER, the oxygen production rate stayed constant throughout the experiment (Figure 2b).

The general decaying trend of the XRR curve over the whole experiment together with the reflectivity switching behavior under potential pulsing is due to progressing surface roughening, as in the case of fast potential cycling. Interestingly, in this case the activity of the surface towards the HER is decreasing. This is likely related to the oxidation at higher potentials and formation and subsequent reduction of a thick 3D oxide. Such cycling can lead to a loss of HER activity and accelerated dissolution of the surface.[33,41,42]

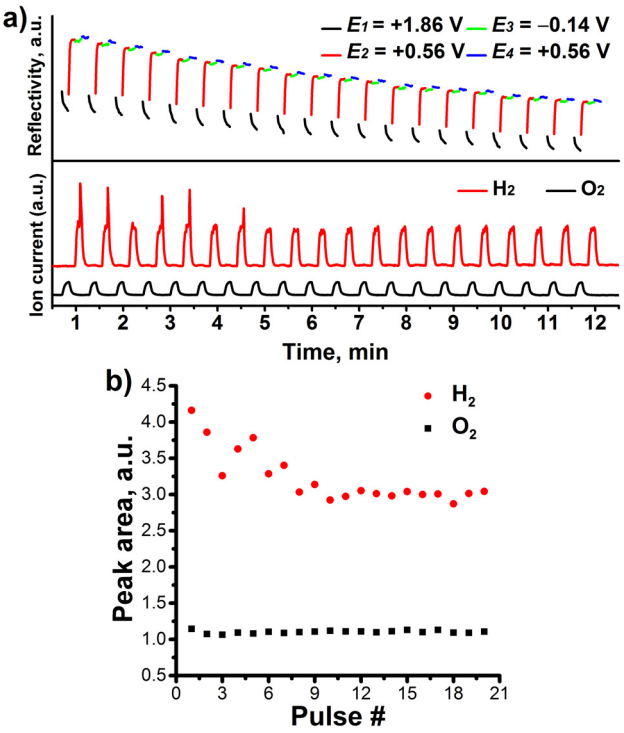

Figure 2. a) Simultaneous XRR ($Q_z = 0.4$ Å^{-1}) (top) and OLEMS (bottom) signals vs. time of the Pt model electrode under the roughening potential pulse sequence; b) amount of produced H_2 and O_2 determined by peak area of OLEMS signals at $m/z = 2$ and $m/z = 32$.

Surface roughening by slow potential cycling followed by *operando* XRR-OLEMS

To demonstrate the scope of the *operando* capabilities of the combined SXS-OLEMS setup, we subjected a UHV cleaned Pt model electrode to CV cycling at slow scan rate while simultaneously recording OLEMS and 1-point XRR ($Q_z = 0.4$ Å^{-1}) response. For this purpose, the Pt model electrode was subjected to a series of 5 slow CVs swept in the range of [–0.14 V to +1.86 V, 10 mV/s] used earlier in this study.

The resulting XRR-OLEMS plots (only first CV cycle shown here) can be divided into 5 potential regions (R-1…R-5) based on the changes in reflectivity along with gaseous product formation (Figure 3a). Starting from open-circuit potential (+0.56 V), then going through HER (–0.14 V) accompanied by a H_2 peak appearing in OLEMS and sweeping towards positive potentials, the XRR curve reveals no change in intensity until a potential of +1.00 V (region R-1) (Figure 3a, b). Continuing from +1.00 V, the related XRR intensity gradually decreases until the potential reaches a value of +1.45 V (R-2). The noticeable intensity decay in region R-2 of the XRR curve corresponds to the formation of a thin surface oxide layer.[44,45]

Region R-3 is starting from +1.45 V (positive direction) goes through the OER peak (+1.86 V) and returns back until +1.64 V in negative direction. In this region, the oxygen evolution reaction takes place, which appears in the form of an increase of the anodic current in the CV and the appearance of

© 2016 Wiley-VCH Verlag GmbH & Co. KGaA, Weinheim

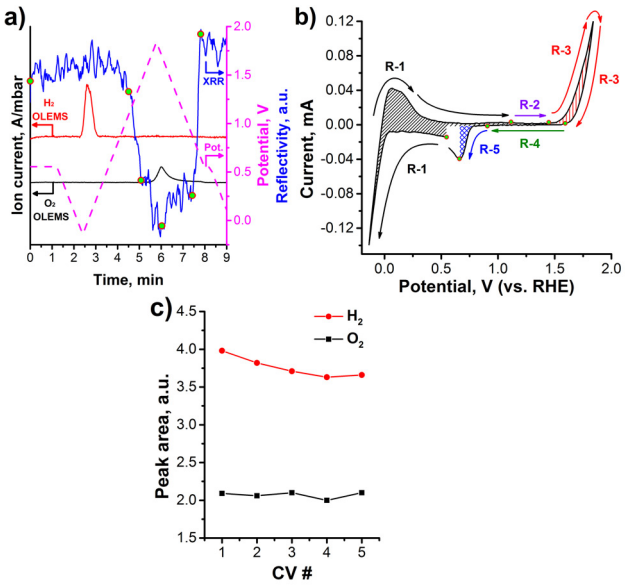

Figure 3. a) *Operando* XRR-OLEMS plot with overlayed potential profile (dashed line) showing change in reflectivity under potential cycling [–0.14 V to + 1.86 V, 10 mV/s] and related H_2 and O_2 OLEMS peaks; b) corresponding cyclic voltammogram; c) integrated area of ion current belonging to H_2 and O_2 OLEMS signals.

the O_2 related OLEMS signal. Meanwhile, there is only a small loss of X-ray reflectivity in the chosen potential range. Further lowering of the potential from + 1.64 V to + 0.92 V, which corresponds in the CV to the featureless electric double-layer (EDL, Region R-4), leads to a slight increase of XRR intensity followed by a sudden jump to its initial high value at + 0.67 V (Region R-5).

Based on the combined XRR-OLEMS-CV dataset described above, the proposed Pt surface transformations can be linked to certain changes in XRR. Starting from the thin oxide region (R-2), rapid thickening of the oxide (33 s, 330 mV) occurs, which points to the active phase of the electrode during OER (R-3). Unlike the oxidation of the Pt, reverse reduction of oxide (25 s, 250 mV) only happens after a long featureless EDL (72 s, 720 mV).

Repeating the roughening CV sequence 5 times reveals similar XRR-OLEMS trends showing the repeatability of the results described above (Figure S7). Integration of OLEMS signals shows a 9% decrease in HER activity, although activity in OER remains unaffected by slow potential cycling (Figure 3c).

Conclusions

The combined SXS-OLEMS datasets of a Pt model electrode demonstrate the ability of our multi-technique approach to obtain simultaneously structure and reactivity trends of electrocatalytic model surfaces under *operando* conditions. Complementary XRR, GISAXS, and SXRD data obtained under identical conditions can provide insight into the structural development of the surface as well as oxide formation, finally arriving at consistent structure-activity relationships for model catalysts recorded under electrochemical *operando* conditions.

The SXS-OLEMS combination will facilitate future studies of electrocatalytic processes on model electrodes leading to comprehensive electrocatalytic structure-activity and potentially structure-selectivity relationships. In addition to electrochemical current and potential data, OLEMS will play to its strength when reactions with a selectivity dimension are studied such as selective (electrocatalytic) oxidation of organic molecules.

Acknowledgements

The authors thank ESRF for technical and financial support during beam times MA1891 and MA2086 at beamline ID03. Also they would like to thank Prof. Marc T. M. Koper from Leiden University for useful discussions. A.G. and E.J.M.H. acknowledge funding by the Dutch National Research School Combination Catalysis Controlled by Chemical Design (NRSC-Catalysis). E.J.M.H. acknowledges support by a TOP grant of the Netherlands Organization for Scientific Research (NWO).

Keywords: Operando · OLEMS/DEMS · Structure-Activity Relationships · Synchrotron · Electrochemistry

[1] K. Sashikata, *J. Vac. Sci. Technol. B Microelectron. Nanom. Struct.* **1991**, *9*, 457–464.
[2] S. Sugawara, K. Itaya, *J. Chem. Soc. Faraday Trans. 1* **1989**, *85*, 1351–1356.
[3] R. Sonnenfeld, P. K. Hansma *Science* **1986**, *232*, 211–213.
[4] V. Climent, J. M. Feliu, *J. Solid State Electrochem.* **2011**, *15*, 1297–1315.
[5] G. Inzelt, R. Holze, H.-H. Strehblow in *Electrochemical Dictionary* (Eds.: A. J. Bard, G. Inzelt, F. Scholz), Springer, Berlin, Heidelberg, **2012**, pp. 666–667; 871–903.
[6] A. J. Bard, L. R. Faulkner in *Electrochemical methods. Fundamentals and Applications*, Wiley-VCH, **2001**, pp. 680–736.
[7] A. T. Hubbard, R. M. Ishikawa, J. Katekaru, *J. Electroanal. Chem. Interfacial Electrochem.* **1978**, *86*, 271–288.
[8] R. M. Ishikawa, A. T. Hubbard, *J. Electroanal. Chem.* **1976**, *69*, 317–338.
[9] P. Christensen, A. Hamnett, *Electrochim. Acta* **2000**, *45*, 2443–2459.
[10] Z. Tian, B. Ren, D. Wu, *J. Phys. Chem. B* **2002**, *106*, 9463–9483.
[11] M. Fleischmann, P. J. Hendra, A. J. McQuillan, *Chem. Phys. Lett.* **1974**, *26*, 163–166.
[12] N. Breuer, A. M. Funtikov, U. Stimming, R. Vogel, *Surf. Sci.* **1995**, *335*, 145–154.
[13] F.-R. F. Fan, A. J. Bard, *Anal. Chem.* **1988**, *60*, 751–758.
[14] M. L. Foresti, A. Pozzi, M. Innocenti, G. Pezzatini, F. Loglio, E. Salvietti, A. Giusti, F. D'Anca, R. Felici, F. Borgatti, *Electrochim. Acta* **2006**, *51*, 5532–5539.
[15] Y. Sun, Y. Ren, D. R. Haeffner, J. D. Almer, L. Wang, W. Yang, T. T. Truong, *Nano Lett.* **2010**, *10*, 3747–3753.
[16] V. P. Tanninen, T. O. Tuomi, *Thin Solid Films* **1982**, *90*, 339–343.
[17] J. Als-Nielsen, D. McMorrow *Elements of Modern X-ray Physics*, Wiley-VCH, **2011**, pp. 69–112.
[18] G. Renaud, R. Lazzari, F. Leroy, *Surf. Sci. Rep.* **2009**, *64*, 255–380.
[19] D. Lützenkirchen-Hecht, H.-H. Strehblow in *Analytical Methods In Corrosion Science and Engineering* (Eds.: P. Marcus, F. B. Mansfeld), CRC Press, **2005**, pp. 169–237.
[20] T. Schülli, V. Favre-Nicolin, M.-I. Richard, G. Renaud, in *Characterization of Semiconductor Heterostructures and Nanostructures* (Eds.: C. Lamberti, G. Agostini), Elsevier, **2013**, pp. 113–173.
[21] F. Golks, K. Krug, Y. Gründer, J. Zegenhagen, J. Stettner, O. M. Magnussen, *J. Am. Chem. Soc.* **2011**, *133*, 3772–3775.

© 2016 Wiley-VCH Verlag GmbH & Co. KGaA, Weinheim

[22] Ch. A. Lucas, N. M. Markovic in *Advances in Electrochemical Science and Engineering*, Vol. 9 (Eds.: R. C. Alkire, D. M. Kolb, J. Lipkowski, P. N. Ross), Wiley-VCH, Weinheim, **2006**, pp. 1–45.
[23] G. M. Bommarito, D. Acevedo, H. D. Abruna, *J. Phys. Chem.* **1992**, *96*, 3416–3419.
[24] A. H. Wonders, T. H. M. Housmans, V. Rosca, M. T. M. Koper, *J. Appl. Electrochem.* **2006**, *36*, 1215–1221.
[25] S. Bruckenstein, R. Gadde, *J. Am. Chem. Soc.* **1971**, *93*, 1966–1967.
[26] H. Baltruschat, *J. Am. Soc. Mass Spectrom.* **2004**, *15*, 1693–1706.
[27] T. H. M. Housmans, A. H. Wonders, M. T. M. Koper, *J. Phys. Chem. B* **2006**, *110*, 10021–31.
[28] Y. Gao, H. Tsuji, H. Hattori, H. Kita, *J. Electroanal. Chem.* **1994**, *372*, 195–200.
[29] J. Greeley, T. F. Jaramillo, J. Bonde, I. Chorkendorff, J. K. Nørskov, *Nat. Mater.* **2006**, *5*, 909–913.
[30] T. Reier, M. Oezaslan, P. Strasser, *ACS Catal.* **2012**, *2*, 1765–1772.
[31] I. Katsounaros, S. Cherevko, A. R. Zeradjanin, K. J. J. Mayrhofer, *Angew. Chemie Int. Ed.* **2014**, *53*, 102–121.
[32] A. Visintin, W. E. Triaca, A. J. Arvia, *J. Electroanal. Chem. Interfacial Electrochem.* **1987**, *221*, 239–243.
[33] A. Iiyama, K. Shinohara, S. Iguchi, A. Daimaru in *Handbook of Fuel Cells* Vol. 5 & 6, (Eds.: W. Vielstich, H. A. Gasteiger, H. Yokokawa), Wiley-VCH, **2009**, pp. 905–915.
[34] A. A. Topalov, S. Cherevko, A. R. Zeradjanin, J. C. Meier, I. Katsounaros, K. J. J. Mayrhofer, *Chem. Sci.* **2014**, *5*, 631–638.
[35] S. Cherevko, G. P. Keeley, S. Geiger, A. R. Zeradjanin, N. Hodnik, N. Kulyk, K. J. J. Mayrhofer, *ChemElectroChem* **2015**, *2*, 1471–1478.
[36] A. A. Topalov, I. Katsounaros, M. Auinger, S. Cherevko, J. C. Meier, S. O. Klemm, K. J. J. Mayrhofer, *Angew. Chemie Int. Ed.* **2012**, *51*, 12613–12615.
[37] H. Angerstein-Kozlowska, B. E. Conway, and W. B. A. Sharp, *J. Electroanal. Chem. Interfacial Electrochem.* **1973**, *43*, 9–36.
[38] B. E. Conway, *Prog. Surf. Sci.* **1995**, *49*, 331–452.
[39] H. Tanaka, Y. Nagahara, S. Sugawara, K. Shinohara, M. Nakamura, N. Hoshi, *Electrocatalysis* **2014**, *5*, 354–360.
[40] K. Yamamoto, D. M. Kolb, R. Koetz, G. Lehmpfuhl, *J. Electroanal. Chem.* **1979**, *96*, 233–239.
[41] H. Imai, K. Izumi, M. Matsumoto, Y. Kubo, K. Kato, Y. Imai, *J. Am. Chem. Soc.* **2009**, *131*, 6293–6300.
[42] M. Matsumoto, T. Miyazaki, H. Imai, *J. Phys. Chem. C* **2011**, *115*, 11163–11169.
[43] T. Erdey-Grúz *Kinetics of electrode processes*, Wiley-Interscience, Budapest, **1972**, pp. 202–242.
[44] H. You, D. J. Zurawski, Z. Nagy, R. M. Yonco, *J. Chem. Phys.* **1994**, *100*, 4699–4702.
[45] Z. Nagy, H. You, *Electrochim. Acta*, **2002**, *47*, 3037–3055.

Submitted: April 11, 2016
Accepted: April 12, 2016

© 2016 Wiley-VCH Verlag GmbH & Co. KGaA, Weinheim